Laser surface texturing of Ti-cp and Ti6Al4V alloy for the improvement of fibroblast adhesion and alignment and the reduction of bacterial adhesion

Journal of Materials Research and Technology 29 (2024) 5464–5472

Contents lists available at ScienceDirect

Journal of Materials Research and Technology

journal homepage: www.elsevier.com/locate/jmrt

Laser surface texturing of Ti-cp and Ti6Al4V alloy for the improvement of fibroblast adhesion and alignment and the reduction of bacterial adhesion

S. Ferraris [a,d,*], A. Cochis [b], A.C. Scalia [b], A. Tori [c], L. Rimondini [b], S. Spriano [a,d]

[a] DISAT Department, Politecnico di Torino – Corso Duca degli Abruzzi, 24 – 10129, Torino, Italy
[b] Department of Health Sciences, Medical School, University of Piemonte Orientale, via Solaroli 17, 28100, Novara, Italy
[c] Osai AS SPA SB (Società Benefit), Via della Cartiera 4, Parella, 10010, Torino, Italy
[d] Interdipartimental Laboratory PolitoBIOMedLab, Politecnico di Torino, Corso Castelfidardo 30A, 10129, Torino, Italy

ARTICLE INFO

Handling editor: P.Y. Chen

Keywords:
Laser
Titanium
Fibroblasts
Bacteria
Contact guidance
Biofilm
Surface

ABSTRACT

Surface texturing is widely investigated for the modulation of the surface properties and biological response of implantable materials. Laser is a green technology for the obtainment of specific patterns without the employment of toxic chemicals. In the present research, a picosecond laser treatment was applied to commercially pure titanium and Ti6Al4V alloy for the obtainment of aligned grooves characterized by micrometric width and spacing but submicrometric depth to promote fibroblast alignment and discourage bacterial adhesion. Surface topography and roughness of laser-textured surfaces were characterized using confocal microscopy, contact profiler, and Scanning Electron Microscopy. Zeta potential titration curves and contact angle measurements were used for the investigation of surface charge and wettability, while X-Ray Diffraction was employed for crystallographic characterization. Finally, the biological response (fibroblast adhesion and alignment and bacterial adhesion) was assessed. Similar results were obtained on commercially pure Ti and Ti6Al4V. Grooves with the designed features were obtained (about 15 μm spaced and 0.2μ deep) and the treated surfaces had a complex micro- and nano-scale morphology which reduced wettability. No evident chemical modification occurred. The treated surfaces were biocompatible and grooves had a contact guidance effect on human fibroblasts. The obtained topography had anti-adhesive action on bacteria (*Staphylococcus aureus*).

1. Introduction

Laser is widely employed in the additive manufacturing of titanium and its alloy for medical applications [1,2] and for the localized treatment of peri-implantitis [3,4]. However, it is gaining increasing interest also for the surface texturing of titanium for obtaining different patterns (e.g. pits, grooves, pillars), roughness, and chemical compositions using different laser-based techniques (e.g. laser ablation, laser-induced periodic surface structures - LIPSSs, laser melting, direct laser interference patterning – DLIP, matrix-assisted pulsed evaporation - MAPLE). One of the great advantages of laser-based techniques is the absence of any surface contact and contamination [5–7]. Moreover, laser is an environmentally friendly technique that does not involve the use of toxic chemicals, it is free from byproducts, and it is characterized by short processing times and reasonable costs [5–7]. Various lasers, such as neodymium-doped yttrium aluminum garnet (Nd:YAG), copper–vapor, Nd:glass (silicate or phosphate glasses), the diode laser, ytterbium-doped laser, and excimer laser, have been used for titanium surface texturing considering impulse applications (with pulse widths of microseconds, nanoseconds, picoseconds, or femtoseconds) or working with a continuous wave [5–7]. Numerous parameters can be varied in laser texturing processes (e.g. focal position, power, number of pulses, energy density – fluency, number of scans, and scanning speed) making it possible to obtain a large variety of surface features [5].

The surface modification of titanium and its alloy is widely investigated in the development of dental implants for supporting the growth of both bone [8,9] and soft tissue [10,11], for successful tissue integration and gum sealing. Parallelly, surface modification can help in reducing the risk of bacterial contamination, which is a significant problem in dental implantology [12].

Laser surface modifications of titanium and titanium alloys have been used for the obtainment of bioactive surfaces (able to induce calcium phosphates precipitation in vitro) [13], to improve protein absorption [14], osteoblast adhesion [15,16], and fibroblasts orientation

* Corresponding author. DISAT Department, Politecnico di Torino – Corso Duca degli Abruzzi, 24 – 10129, TORINO, Italy.
E-mail address: sara.ferraris@polito.it (S. Ferraris).

https://doi.org/10.1016/j.jmrt.2024.03.033
Received 1 December 2023; Received in revised form 28 February 2024; Accepted 5 March 2024
Available online 6 March 2024

[13,17]. A certain ability to reduce bacterial adhesion has also been observed on laser-textured titanium surfaces [17,18]. A significant interest in laser surface texturing has been demonstrated also by dental implant producers, as confirmed by commercial dental implants with laser-treated surfaces aimed at improved bone [19,20] or soft tissue [21] attachment. A reduction of bacterial adhesion on laser-treated dental implants has also been reported [19].

In the present research, a picosecond laser treatment was used to obtain oriented grooves and multiscale texture (micro- and nano-scale) on commercially pure (Ti-cp, grade 2) and Ti6Al4V alloy to improve gingival fibroblasts adhesion and orientation. The main innovation of the present work is related to the combination of groove topography (able to guide cell orientation) and micro/nano features able to support cell adhesion and avoid bacterial one. This combination is possible by a proper design of structures' dimensions. In fact, differently from the research works reported in the literature and from commercial laser modified dental implants, the obtained grooves were characterized by micrometric (15–20 μm) width and spacing but submicrometric depth, making possible the maintenance of an average surface roughness (Ra) lower than 0.2 μm. This is of particular interest for a surface with a low risk of bacterial contamination because it is the threshold, reported in the literature, not to increase bacterial adhesion [22–24]. Moreover, the topography of these grooves is characterized by nanofeatures able to affect cell and bacterial behavior. The eventual effect of the nano-scale topography on reducing bacterial contamination was also investigated.

2. Materials and methods

2.1. Samples preparation

Square samples (1 × 1 cm), 1 mm thick, were cut from a sheet of commercially pure titanium grade 2 (ASTM B265-13A, annealed, Titanium Consulting and Trading) or Ti6Al4V (grade 5, ASTM B265, annea led, Titanium Consulting and Trading). Samples were mechanically polished with SiC abrasive papers up to 4000 grit and then washed once in ethanol for 5 min and twice in ultrapure water for 10 min in an ultrasonic bath. Mechanically polished samples will be designed as Ti-cp - MP and Ti6Al4V – MP from now on.

2.2. Laser surface texturing

A picosecond 100 W IR (infrared) laser system (HyperRapid NX model, Coherent, Germany) with a Galvo scanner head was used for the surface texturing of Ti-cp and Ti6Al4V samples.

Texturing was performed in air with a frequency of 500 kHz, a selected power of 20 W and a scanning speed of 1000 mm/s as optimized parameters for the obtainment of the desired grooves on Ti-cp and Ti6Al4V.

Laser-treated samples will be designed as Ti-cp - L and Ti6Al4V – L from now on.

2.3. Physical and chemical surface characterization

Surface topography and roughness were investigated using confocal microscopy (Zeiss LSM 900, Oberkochen, Germany, 20×/0.95×objective and 10× further magnification from camera) and contact profilometry (Intra Touch, Taylor Hobson, Leicester, United Kingdom). A representative area per each type of sample was observed by confocal microscopy. At least 3 line profiles were measured, for each sample type, by contact profilometry. Roughness parameters were obtained according to the ISO4287 standard using the instrument software (TailyMap). Data have been analyzed by means of one-way ANOVA, with a significance level $p < 0.05$.

Surface morphological features, such as micro-grooves and nano-texture, were observed using Scanning Electron Microscopy (SEM, JEOL, JCM 6000 plus) and Field Emission Scanning Electron Microscopy (FESEM – SUPRA™ 40, Zeiss) respectively, both equipped with Energy Dispersive Spectroscopy (EDS) for chemical semi-quantitative analyses. SEM was sufficient for imaging up to 10000×, useful for the detection of grooves and micrometric features, while FESEM was necessary for the proper investigation of nanometric features.

The crystalline structure was studied through X-Ray Diffraction (XRD) in Bragg-Brentano configuration (XRD – PANalytical X'Pert Pro PW 3040160 Philips, Malvern Panalytical, Egham, United Kingdom) and the patterns were analyzed by XPERT High Score software.

Surface wettability was investigated through static contact angle measurements (DSA-100, KRÜSS GmbH, Hamburg, Germany) using ultrapure water as a wetting fluid. A drop of ultrapure water (5 μl) was deposited on the surface of the sample and the contact angle with the surface was measured by the instrument software (DropShape Analysis). At least 3 measurements for each surface type were acquired.

The zeta potential in the function of pH was measured through an electrokinetic analyzer (SurPASS, Anton Paar) equipped with an adjustable gap cell. A solution of 0.001 M KCl was used as an electrolyte and its pH was adjusted by the addition of 0.05 M HCl for acid titration and 0.05 M NaOH for basic titration through the instrument's automatic titration unit. The same set of samples was used for basic and acid titrations, running the basic one first, followed by copious rinsing, and finally by the acid titration.

2.4. Biological characterizations

2.4.1. In vitro cytocompatibility evaluation

2.4.1.1. Cells cultivation. Human fibroblasts were used to assay specimens' cytocompatibility. Cells were purchased from the American Type Culture Collection (ATCC, VA, USA, CRL-4061) and cultivated using the alpha-modified minimal essential medium (α-MEM, from Sigma-Aldrich, Milan, Italy) supplemented with 10% fetal bovine serum (FBS, Lonza, Milan, Italy) and 1% antibiotics (penicillin/streptomycin) at 37 °C, 5% CO_2. When cells reached 80–90% confluence, they were detached by trypsin/EDTA solution, collected, and used for experiments.

2.4.1.2. Direct cytocompatibility. Specimens were heat sterilized at 180 °C for 1 h in a dry oven before biological tests. Sterile specimens were gently seeded to a new 12-multiwell plate by sterile tweezers avoiding any surface damage. Then, a defined number of cells (1×10^4 cells/specimens) were dropwise (100 μl) seeded directly onto the specimens' surface and allowed to adhere for 2 h at 37 °C, 5% CO_2. Afterward, each well was rinsed with 1 ml of fresh medium, and the cells were cultivated for 24-48-72 h. At each time-point, specimens were first moved to a new multiwell plate, and then cell viability was verified using metabolic activity by the metabolic colorimetric Alamar blue assay (alamarBlue®, ThermoFisher, Waltham, MA, USA) following the manufacturer's instructions. Briefly, at each time-point, supernatants were removed from each well-containing cell and replaced with Alamar blue solution (10% v/v in fresh medium). Plates were incubated in the dark for 4 h and then 100 μl were removed, spotted into a new black 96-well plate and fluorescence signals were evaluated with a spectrophotometer (Spark, from Tecan Trading AG, Switzerland) using the following set-up: fluorescence excitation wavelength 570 nm, fluorescence emission reading 590 nm. As a control, the Alamar solution in contact with test materials solely (intended as cells-free) was applied and compared with the fluorescence of the same solution to exclude any reading background due to the reactive groups on the surface. Results were expressed as relative fluorescence units (RFU).

2.4.1.3. Morphological analysis. After 72 h in culture, the morphology of seeded cells was visually checked by Fluorescent Imaging (IF) and SEM. For IF staining, cells were fixed at room temperature by Immunofix solution (Bio Optica, Milan, Italy) for 15min; then, they were washed 3

times with phalloidin (ab176759, AbCam, Cambridge, UK) and 4′,6-diamidino-2-phenylindole (DAPI, Sigma-Aldrich, Milan, Italy) to visualize cytoskeleton f-actin filaments and nuclei, respectively.

For SEM imaging, specimens were fixed overnight in 4% glutaraldehyde (from Sigma-Aldrich, Milan, Italy, 4 °C, diluted in cacodylate buffer) and then dehydrated by the alcohol scale (50-70-90-100%, 1 h each). Then, samples were treated in hexamethyldisilazane (Sigma-Aldrich, Milan, Italy) for 20 min at room temperature, mounted onto aluminum stubs with conductive carbon tape to undergo surface metallization through a gold layer, and observed with a JSM-IT500 SEM using secondary electrons (from Jeol S.P.A., Basiglio, Italy).

2.4.2. *In vitro antibacterial activity*

2.4.2.1. Strain growth conditions. Specimens' antibacterial or anti-fouling properties were tested against the pathogen, strong biofilm former, and multi-drug resistant strains *Staphylococcus aureus* (*S. aureus*, ATCC 43300). Bacteria were cultivated in Trypticase Soy Agar plates (TSA, Sigma-Aldrich, Milan, Italy) at 37 °C until round single colonies were formed; then, 2–3 colonies were collected and spotted into 30 ml of Luria Bertani broth (LB, Sigma-Aldrich, Milan, Italy). Broth cultures were incubated overnight at 37 °C in agitation (120 rpm in an orbital shaker), then they were diluted with fresh medium till a final optical density of 0.001 at 600 nm was reached corresponding to a final number of 1×10^5 cells/ml as previously described [25].

2.4.2.2. Antibacterial evaluation. Bacteria at the final concentration of 1×10^5/specimen [26] representative for acute infection in bone-related models [27,28] were directly seeded onto the surface of the specimens and allowed growth for 90 min or 24 h at 37 °C in an incubator with 5% CO_2 and 95% humidity allowing for biofilm formation [29]. Afterward, specimens were collected, carefully washed 3 times with sterile PBS to remove non-adherent cells, and seeded into a new plate. The number of viable colonies adhered to the specimens' surface was determined by the colony-forming unit (CFU) count; specimens were moved to tubes containing 1 ml of PBS, and the biofilm was detached from specimens by sonicator and vortex (30 s, 3 times each). Then, 100 μL of supernatant were collected from each tube and used to perform six serial 10-fold dilutions, by mixing 20 μL of bacterial suspension with 180 μL of sterile PBS. Twenty microliters (1/10 of the 200 μl contained in each well after the dilution) were then collected from each dilution, spotted onto plates containing LB agar medium, and incubated for 24 h at 37 °C. Lastly, the CFU/ml were counted as previously detailed by the Authors [30].

Finally, the morphology and the biofilm-like 3D structures of the adhered bacteria were investigated by SEM as previously described.

2.4.3. *Statistical analysis of data*

Biological assays were performed in triplicate. Groups were compared by the one-way ANOVA using Tukey's test as a post-hoc analysis. Significant differences were established at $p < 0.05$.

3. Results and discussion

3.1. *Physical-chemical characterization*

Topographical images obtained using confocal microscopy and roughness parameters measured by contract profilometry on the treated surfaces (Ti-cp-L and Ti6Al4V-L) are shown in Fig. 1. As a reference, the images and the values obtained by contact profilometry on smooth

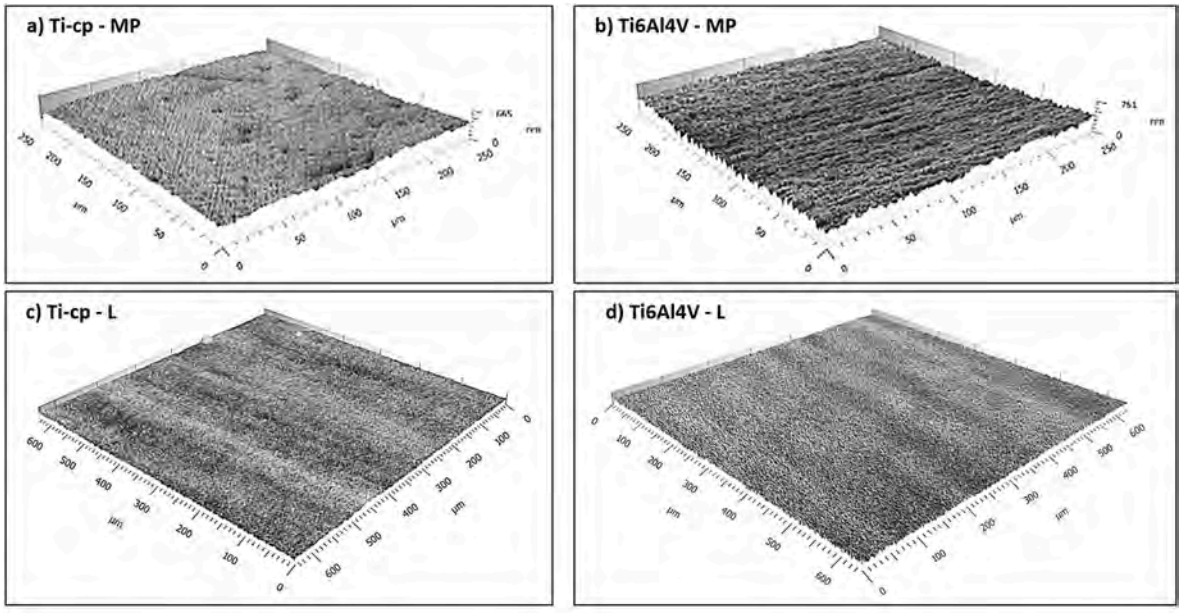

e)	Ti-cp - MP	Ti-cp - L	Ti6Al4V - MP	Ti6Al4V - L
Ra [μm]	0.037±0.004	0.198±0.002	0.052±0.001	0.207±0.007
Rz [μm]	0.383±0.043	1.5±0.06	0.387±0.033	1.57±0.116
Rsk	-1.5±0.227	-0.075±0.059	-0.416±0.108	-0.058±0.164
Rku	7.113±1.089	2.973±0.145	3.01±0.337	2.853±0.03

Fig. 1. Topographical images obtained by confocal microscopy of (a) Ti-cp – MP (200× mag.) (b) Ti6Al4V – MP (200× mag.), c) Ti-cp – L (200× mag.) and d) Ti6Al4V – L (200× mag.). (e) Roughness parameters obtained by contact profilometry.

(mechanically polished) surfaces are also reported (Ti-cp-MP and Ti6Al4V-MP).

Aligned grooves with a few tens of microns spacing were clearly visible on both surfaces confirming the effectiveness of laser texturing.

As expected, the mean roughness (Ra) was very low on Ti-cp-MP and Ti64-MP (0.037–0.052 μm) and higher, ≈0.2 μm, for Ti-cp-L and Ti6Al4V-L. The difference between the Ra values of MP and corresponding L sample was statistically significant ($p < 0.05$). This was the first indication that the produced surfaces were in line with the initial design: roughness was lower than the threshold (0.2 μm) reported in the literature for not increasing bacterial adhesion [22–24]. Even if Ra is a widely used reference value, several topographical parameters are needed to describe in detail a surface [26]. Rz values are sensitive to the highest peaks and lowest valleys [31] and an increase in these values was observable after laser texturing due to the appearance of grooves and holes typical of laser treatments. Also the difference between the Rq values of MP and corresponding L sample was statistically significant ($p < 0.05$). Skewness (Rsk) describes the symmetry of the profiles around the mean line [31], in particular, negative values are measured on surfaces characterized more by valleys than by asperities, while positive values are representative of surfaces with the opposite [31]. Mechanically polished and laser-textured surfaces typically show negative skewness values because they come from subtractive treatments. The experimental values obtained on Ti-cp-L and Ti6Al4V-L were negative, as expected. Finally, kurtosis (Rku) describes the distribution of peaks and valleys in height (a measure of the peakedness of the profile). Values higher than 3 indicate the presence of sharp surface features (many peaks and/or valleys with pointed morphology), while values lower than 3 indicate a surface with negligible presence of sharp peaks and deep valleys and a more smoothed morphology of surface features. Values close to 3 indicate a Gaussian distribution in the height of peaks and valleys [31]. Except for Ti-cp – MP, the measured Rku values are close to 3. This can be explained by the low hardness of Ti-cp which was deeply engraved during the polishing procedure. In fact, the high values of Rsk and Sku for this surface can be explained its low surface hardness and the unavoidable presence of polishing defects. On the other hand, the here optimized laser surface texturing is able to produce surfaces with sub-micrometric oriented grooves without sharp peaks and deep valley and with a smoothed morphology, which is not so common for laser textured titanium alloys [32]. In conclusion, a texture with a negative asymmetry (Rsk) and Gaussian peak distribution in height (Rku) can be beneficial for cell adhesion, as it was on Ti-cp-L and Ti6Al4V-L, while sharp asperities could discourage cell adhesion [7–11].

The surface morphology of the treated surfaces (Ti-cp-MP and Ti6Al4V-L) is shown, by SEM/FESEM images at different magnifications, in Fig. 2.

At low magnification (400×, Fig. 2a–e) grooves about 15 μm spaced are visible on Ti-cp-L and Ti6Al4V-L. Due to their limited depth (≈0.2 μm, as estimated from roughness measurements - Fig. 1c), dashed half lines have been introduced to facilitate their detection on the image. The low depth of these grooves is one of their main difference from laser surface textures actually employed in biomedical applications. Increasing the magnification at 1000× (Fig. 2b–f) a periodic structure of a few microns is evident on both laser-treated surfaces. The main width of these structures (see arrows in Fig. 2 c and g) is between 0.75 and 1.70 μm. At higher magnifications (10000× and 100000× Fig. 2c, d, g, and h) globule-like nanofeatures (50–200 nm) are visible on the micrometric periodic structures. In conclusion, the designed grooves were obtained and the treated surfaces have a complex morphology with features at the micro-and nano-scales.

XRD spectra of commercially pure Titanium and Ti6Al4V alloy before and after laser texturing are reported in Supplementary Fig. S1. All the peaks can be assigned to alpha titanium (reference pattern 00-044-1294). As previously observed by the authors [33], peaks of beta titanium are usually evident for Ti6Al4V alloy only after bulk thermal treatments. Laser texturing induces a local surface heating which does not affect the bulk material structure nor in terms of beta titanium formation nor in terms of deep oxidation, only a thin surface oxidation layer can be supposed, as described in the following. Moreover, no martensite formation can be observed on these specific laser-textured samples, differently from what often occurs on titanium surfaces treated by laser or electron beam [33,34].

The contact angle of ultrapure water on mechanically polished surfaces was 60.3 ± 8.0° for Ti-cp and 72.4 ± 1.8° for Ti6Al4V, in line with the values reported in the literature for the same materials [35,36]. After laser texturing an increase of the contact angle can be registered on both surfaces, in fact, values of 70.33° ± 7.5° and 84.76° ± 2.2° have been measured on Ti-cp – L and Ti6Al4V – L, respectively. A discussion of these values is reported later considering the measured zeta potential titration curves, too.

Zeta potential titration curves of commercially pure titanium and Ti6Al4V alloy before and after laser texturing are reported in Fig. 3. These curves gave information about the isoelectric point, chemical reactivity of surface functional groups, and wettability. Moreover, the standard deviation of the measurement gives indication about surface stability at the tested pHs [37].

The isoelectric points of Ti-cp - MP and Ti6Al4V - MP were 4.09 and 3.68, in line with the values reported in the literature [38,39] for surfaces without specific functional groups with acidic/basic behavior [40]. After laser texturing, a moderate shift toward more basic values

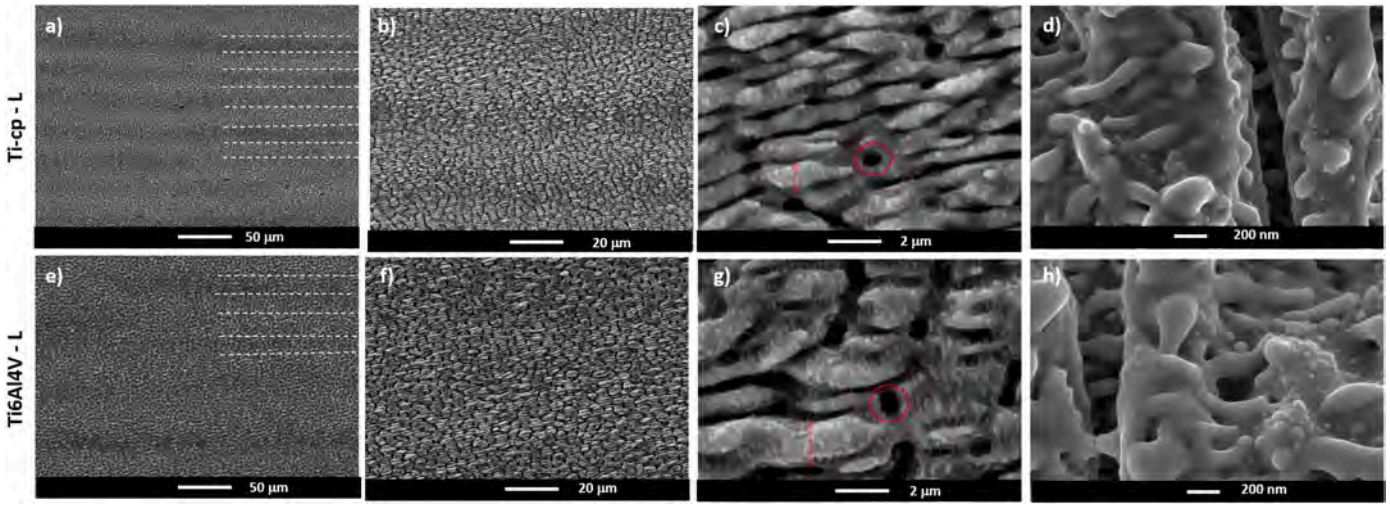

Fig. 2. SEM/FESEM images of Ti-cp – L surface (a–d), SEM/FESEM images of Ti6Al4V – L surface (e–h).

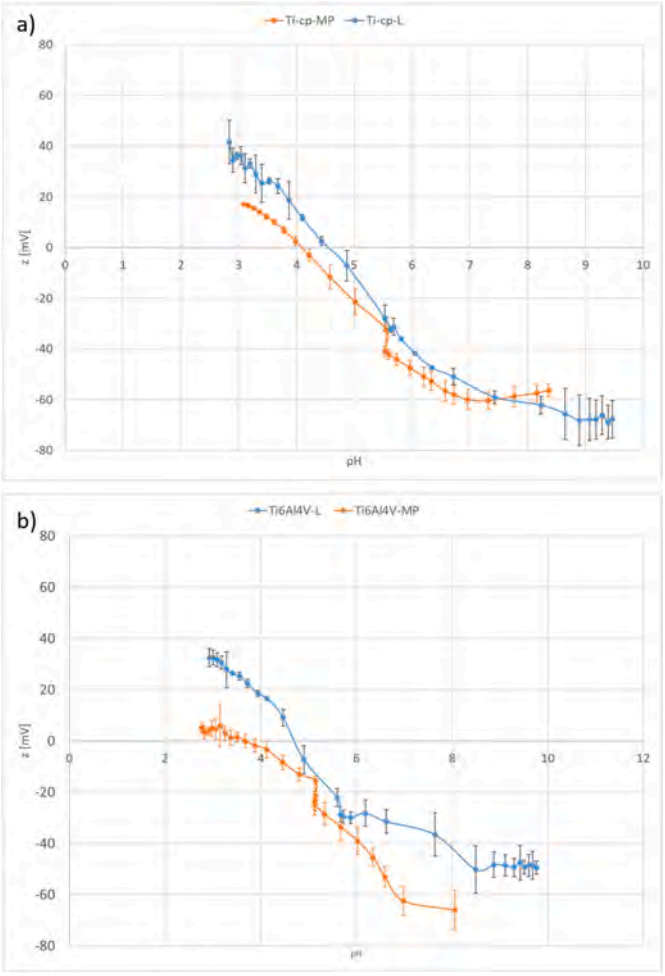

Fig. 3. Zeta potential titration curves of a) commercially pure titanium before and after laser texturing, b) Ti6Al4V before and after laser texturing.

(4.55 for Ti-cp – L and 4.71 for Ti6Al4V – L) was observed: the formation of an oxide layer with a slight prevalence of basic OH groups can be supposed. The laser texturing is performed in air and induce a local increase of the temperature, in these conditions a certain surface oxidation is expected and confirmed by surface coloring typical of titanium oxides. All the surfaces are expected to be negatively charged at physiological pH. On the other hand, the laser-textured surfaces had a slight positive charge at inflammatory pH (4–5), differently from the mechanically polished ones. Two small plateaux, one in the acidic range, with an onset close to 3, and one in the basic range, with an onset at 8.5 can be observed. They can be associated with the formation after laser texturing of an oxide layer with OH groups with respectively low basic or acid strength, completely protonated/deprotonated only at very high/low pHs. Considering the slope of the curve around the isoelectric point, which is correlated with surface wettability [40], it is not significantly altered after the treatment, suggesting that the increase in the contact angle observed in the wettability tests is mainly related to topographic factors and not to chemical ones. This means that no hydrophobic species are introduced on the surface by the laser treatment, as expected.

Looking at the standard deviations of the measurements it can be observed that they are very small, supporting a high stability of the surfaces in the tested pH range.

3.2. Biological characterizations

3.2.1. Cytocompatibility evaluation

After the laser-assisted surface modification, the cytocompatibility of the developed materials was tested as the first biological property. As previously shown in Fig. 2 by FE-SEM imaging, the obtained surfaces' topography resembles a well-oriented topography that can be hypothesized as influencing/guiding cells in the early adhesion phase. This contact-guidance effect can be of particular interest for implantable biomaterials such as dental abutments, where the success of the implant is strongly related to the mechanical stability of the device-gingiva sealing. In fact, the tight connection between cells and the device's surface represents a key factor protecting the implant from harmful micro-oscillations by the extracellular matrix deposition [41]; moreover, a strong tissue-device connection can efficiently prevent bacterial adhesion and colonization, a devasting event that can bring to the implant failure if bacteria can move to the bone site where the screw supporting the abutment is surgically inserted a few months earlier [42]. Based on these premises, we selected to use human gingival fibroblasts (HFG) for the tests, as cells representative for the gingiva connecting to the abutment, and a focus was put on the Ti6Al4V substrate because it has large employment for abutments [43]. As a confirmation, such bulk surfaces can be considered as positive controls to rank the cytocompatibility of the laser-modified ones because the metabolic activity of HFG cells cultivated onto their surfaces is comparable to that one reported by the same cells cultivated onto the gold-standard polystyrene as reported in the Supplementary Fig. S2.

Results are reported in Fig. 4. In general, the laser surface treatment did not introduce any toxic elements or compounds as the metabolic activity of HGF cells cultivated onto laser-treated specimens (Ti6Al4V – L) was not significantly reduced in comparison to the bulk Ti6Al4V – MP at all the tested 24-48-72 h' time-points ($p > 0.05$, Fig. 4 a). Accordingly, the viability of the surface-seeded cells was always >70% in comparison to the Ti6Al4V – MP that was considered as 100% viability as previously discussed (Figs. 4 b, 100% is represented by the dashed line). Finally, fluorescent images (Fig. 4 c) and SEM pictures (Fig. 4 d) collected after 72 h of direct cultivation showed a comparable elongated fibroblast-like shape of the cells cultivated onto both the samples (cytoskeletons are stained in red by phalloidin) as well as the cells adapted to the modified topography thus well adhering onto the laser-modified surfaces, confirming the data obtained through metabolic evaluation. To further confirm that the laser treatment can be considered a safe procedure, the Ti-cp substrate has been laser modified (Ti-cp – L) and compared to Ti6Al4V – L. Results are reported in Supplementary Fig. S3 and no significant differences were noticed between the two groups in terms of metabolic activity (Supplementary Fig. S3 a-b) and morphology by fluorescent (Supplementary Fig. S3c) and SEM (Supplementary Fig. S3d) images. In conclusion, the laser-treated titanium surfaces were confirmed as cytocompatible. It is interesting to note that the increased hydrophobicity, due to the multiscale topography, did not negatively impact cell adhesion as it usually occurs when it is related to surface chemistry and hydrophobic compounds.

3.2.2. Cells' alignment

After verifying that the laser treatment did not introduce any toxic elements affecting cells' viability in direct contact with specimens, we then focused on the ability of the introduced topography to provide a contact-guidance effect to the adhered cells. In general, the surface modification of implantable materials represents a promising strategy to improve the adhesion of the ingrowing tissue to the implant as reported by a large literature [44–46]. In this specific case, gingival fibroblasts were stimulated to colonize a new surface by an oriented topography resembling the alignment that they reach when they tightly attach to the abutment [45,47]. In this research, grooves highly oriented and aligned to each other in a parallel manner were obtained by laser surface treatment, thus resembling an ideal topography to drive gingival

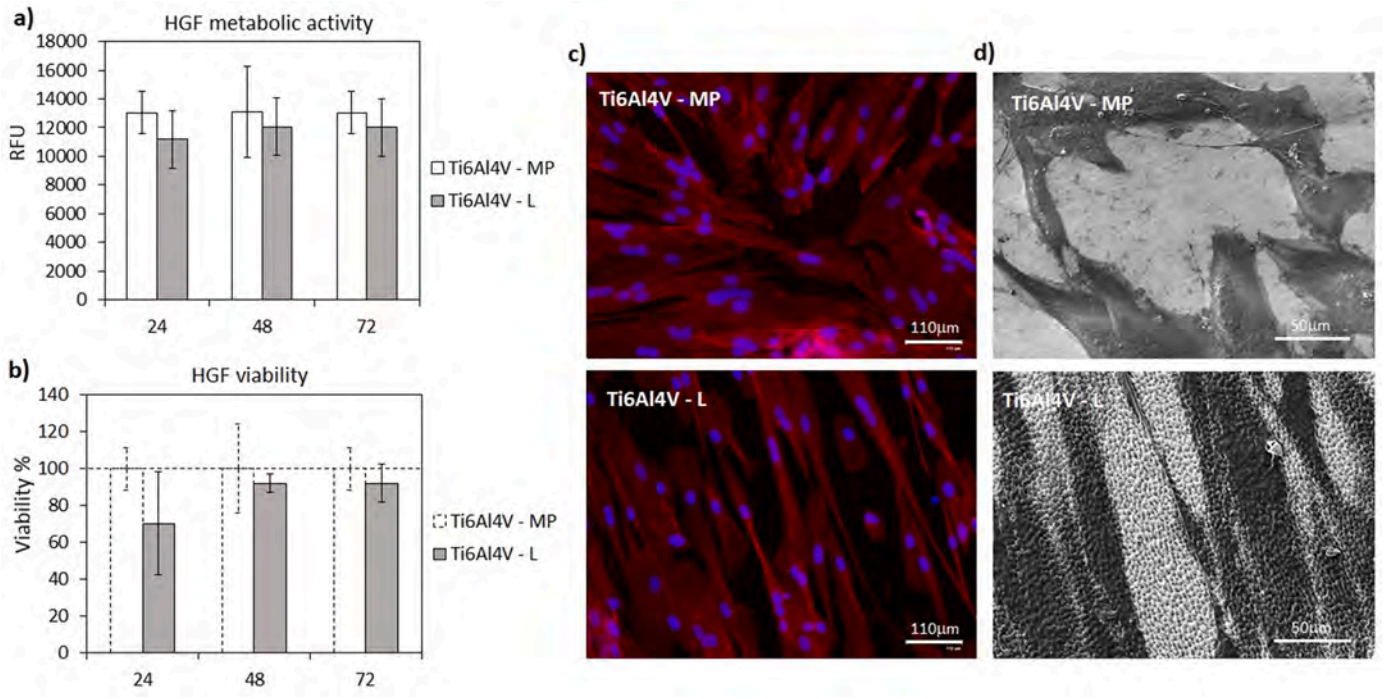

Fig. 4. Cytocompatibility. **(a)** The metabolic activity of HGF cells cultivated onto laser-treated surfaces (Ti6Al4V – L) did not report any significant decrease in comparison to the control Ti6Al4V – MP ($p > 0.05$); **(b)** accordingly, the viability of the cells was between 70 and 99% if compared to the control considered as 100% (indicated by the dashed lines). **(c)** Fluorescent imaging demonstrated a comparable elongated morphology of the cells cultivated onto both substrates (cytoskeletons are stained in red and nuclei in blue), as well as **(d)** SEM images demonstrated that cells adapted to the nano-topography of the laser-treated surfaces. Bars represent means ± dev.st of 3 replicates. (For interpretation of the references to color in this figure legend, the reader is referred to the Web version of this article.)

fibroblast adhesion and alignment by contact guidance. Therefore, HGF morphology was visually checked by fluorescent imaging (cytoskeleton F-actin filaments marked in red by phalloidin and nuclei in blue by DAPI) and scanning electron microscopy (SEM) after 72 h of cultivation; results are reported in Fig. 5.

As expected, HGF cells cultivated onto polished surfaces (Ti6Al4V – MP) reported a physiological elongated morphology resembling fibroblasts, but their orientation was mostly random (Fig. 5 a, left panel). On the opposite, when the cells were cultivated on laser-treated surfaces (Ti6Al4V – L), an evident orientation was observed by fluorescent images of different regions of the specimens (Fig. 5 a, right panel, the orientation is suggested by the white arrows). To clarify whether such orientation was due to the surface topography, SEM images were collected (Fig. 5b, upper and lower panels) and the hypothesis was confirmed by the evidence that the cells' cytoskeleton spread was guided by the grooves. In fact, lower magnification images (upper panel) confirmed fluorescence ones suggesting for an oriented cells' orientation, but by the higher magnification SEM images (lower panel) it can be appreciated that such shape is directly driven by the grooves imposing a cytoskeleton arrangement following the surface topography. As previously done for cytocompatibility, the contact guidance effect was verified on the Ti-cp-L surface that was compared to Ti6Al4V-L. Results are reported in Supplementary Fig. S4, confirming that the same orientation was achieved for the Ti-cp-L specimens too, suggesting a wide exploitation of the laser to modify implantable metals' surfaces.

The contact-guidance effect does not represent a novelty, as it is well known that surface topography can influence cells' orientation, but in this case, the suitability of the laser procedure was demonstrated. Laser-treatment of titanium allows to obtain instructive surfaces able to improve the gum adhesion around the abutment. The design of the grooves is of great relevance to get the contact guidance effect. The grooves' geometry (spacing and depth) designed in this research and the obtained topography were successful in all the required steps: fibroblast adhesion, inter-cellular communication, and alignment. The obtained asymmetric, negative, and rounded topography was favorable to a good response from fibroblasts: cytocompatibility and cell alignment.

3.2.3. *Antibacterial efficacy*

Bacterial infections nowadays represent a major reason for implant failure due to their ability to fast colonize the surgical site and to resist the majority of the clinically-exploited antibiotics [48,49]. In dentistry, the teeth substitution by artificial implant requires typically a 2-step surgery: first, the screw is implanted into the bone and then, usually, after 3 months during which osteointegration occurs, a flap of the gingiva is surgically created to allow the abutment connection to the screw. In this second stage, a tight sealing between the gingiva and the abutment, immediately after surgery, plays a pivotal role and a physical hurdle for bacteria that are unable to move toward the bone compartment [50]. However, the complete sealing requires some days in which bacterial infection can occur. It would be very important that the abutment itself is able to prevent the adhesion of bacteria or their proliferation while closing the seal with the gum. In this view, micro- and nano-topographies- represent a promising approach since their particular structures can prevent bacterial adhesion by reducing the anchorage sites as well as they can bring bacteria death due to the irreversible damage occurring to the membranes when bacteria try to adapt to the surface irregularities as reported also by the authors [26,34,51]. Here, the laser treatment was effective in producing irregular nanotopographies, therefore the adhesion of bacteria at an early stage (90 min) as well as their proliferation at a late time point (24 h) were tested in direct contact with the specimens: results are summarized in Fig. 6.

In the early 90 min (90 min, adhesion step), a reduced number of bacteria was counted by the CFU assay onto the laser-modified surfaces Ti6Al4V - L in comparison to the polished Ti6Al4V – MP control (Fig. 6 a). As expected, both counts were below the starting number of bacteria (1×10^5 bacteria/specimen) as the majority of them belong to the non-adherent planktonic part; however, the evidence that the presence of the

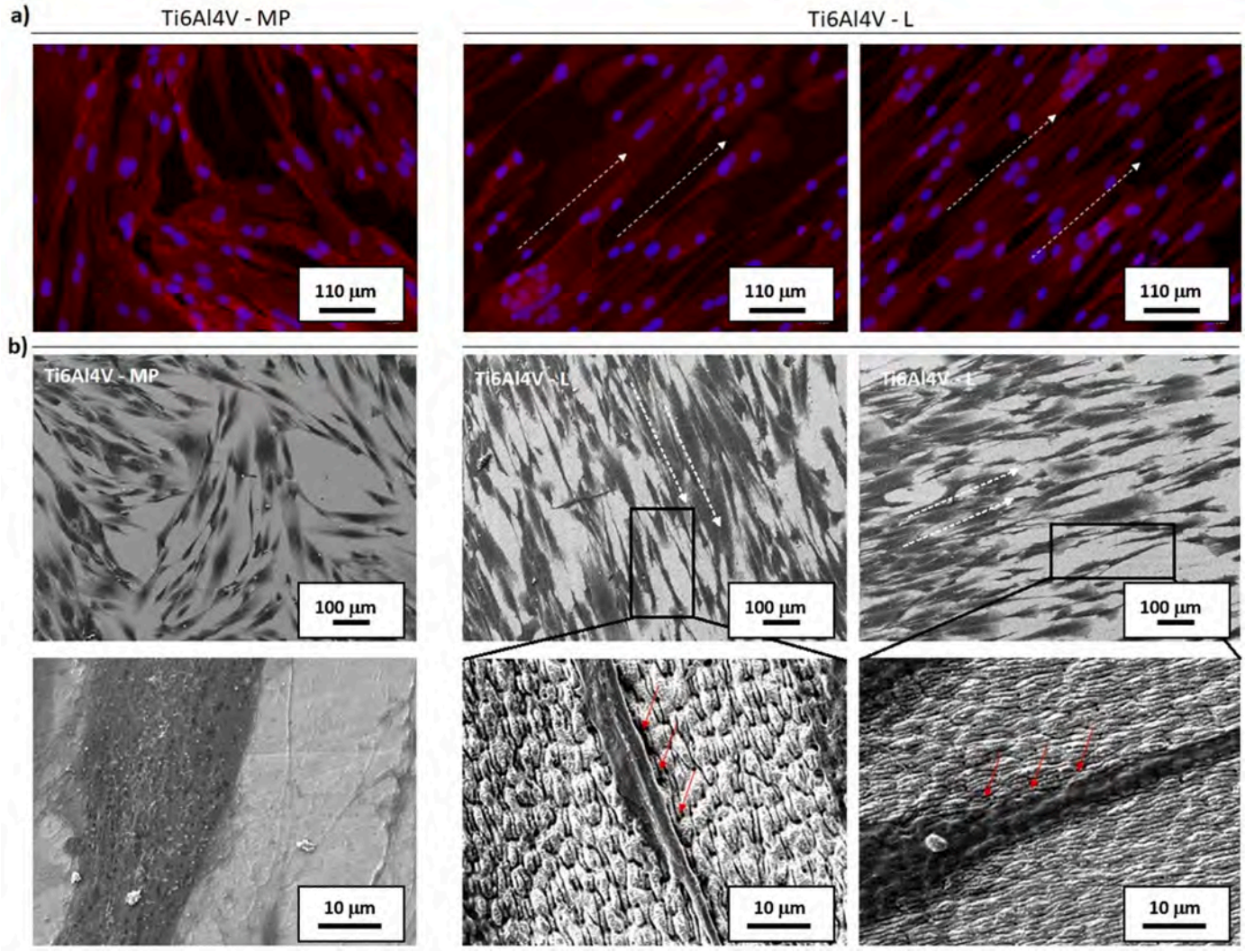

Fig. 5. Cells' alignment. **(a-b, left panels)** HGF cells cultivated onto untreated Ti6Al4V – MP control surfaces correctly adhered but following a random orientation; **(a-b, right panels)** on the opposite, cells seeded onto laser-modified Ti6Al4V – L surfaces were guided to an oriented conformation (suggested by the white arrows) as can be seen in the lower magnification images on the top panel due to the surfaces' grooves influencing cytoskeletons' arrangement as reported in the higher magnification images in the bottom panel of the SEM images.

grooves further reduced the number of adhered bacteria in comparison to the bulk MP specimens represents a confirmation that bacteria are less prone to adhere due to the lower number of anchorage points. More interestingly, a statistically significant difference in terms of viable bacteria colonizing surfaced was noticed by comparing Ti6Al4V – L with the control Ti6Al4V – MP (Fig. 6 a, $p < 0.05$ indicated by #) after 24 h of infection. In fact, the number of bacteria colonizing Ti6Al4V – MP increased by 19.3× in the time range between 90 min and 24 h, whereas on Ti6Al4V – L the starting number was increased by 3.8×. Such difference was evident when SEM images were collected after 24 h (Fig. 6 b), showing many bacteria growing randomly and forming multi-colonies aggregates homogeneously distributed on the surface of Ti6Al4V – MP (left panel). On the opposite, only a few random colonies were found on Ti6Al4V – L, mostly showing single colonies conformation (right panel). SEM images was selected to show these aggregates derived from the ability of bacteria to proliferate without any impediment, representing the bulk structure of the biofilm that was much more frequently observed on the surface of the Ti6Al4V – MP than to the Ti6Al4V – L ones as reported in the Supplementary Fig. S5. Finally, Ti-cp - L was tested for its antibacterial properties following the same scheme as Ti6Al4V – L to further confirm the suitability of the laser to modify implantable materials. Results are reported in Supplementary Fig. S6, showing comparable values ($p > 0.05$) between the two groups thus demonstrating the possibility of modifying different titanium surfaces with a laser to confer antibacterial properties.

The ability of the nano-topography to prevent bacteria expansion into biofilm-like 3D aggregates was well discussed by Sorzabal-Bellido et al. [52]. They developed an algorithm defining that bacteria can grow/progress following precise 90-180-45° directions. According to this hypothesis, the topography obtained in this research represented a physical hurdle to the bacteria growth linear progression, thus preventing biofilm formation. First, the designed grooves had a geometry suitable to be not a niche for bacteria. Furthermore, the multiscale topography generated by the laser treatment was effective in behaving like a hurdle for bacteria and turned out as an interesting strategy for antibacterial implants with a reduced risk of colonization.

The favorable anti-adhesive effect of textured surfaces has been previously hypothesized through numerical modeling evidencing that surface features smaller than bacterial cells can effectively prevent adhesion [53]. The presence of functional groups with a basic/acid chemical reactivity, with a small prevalence of the basic ones, could also play a minor role in the antibacterial effect introducing some positively

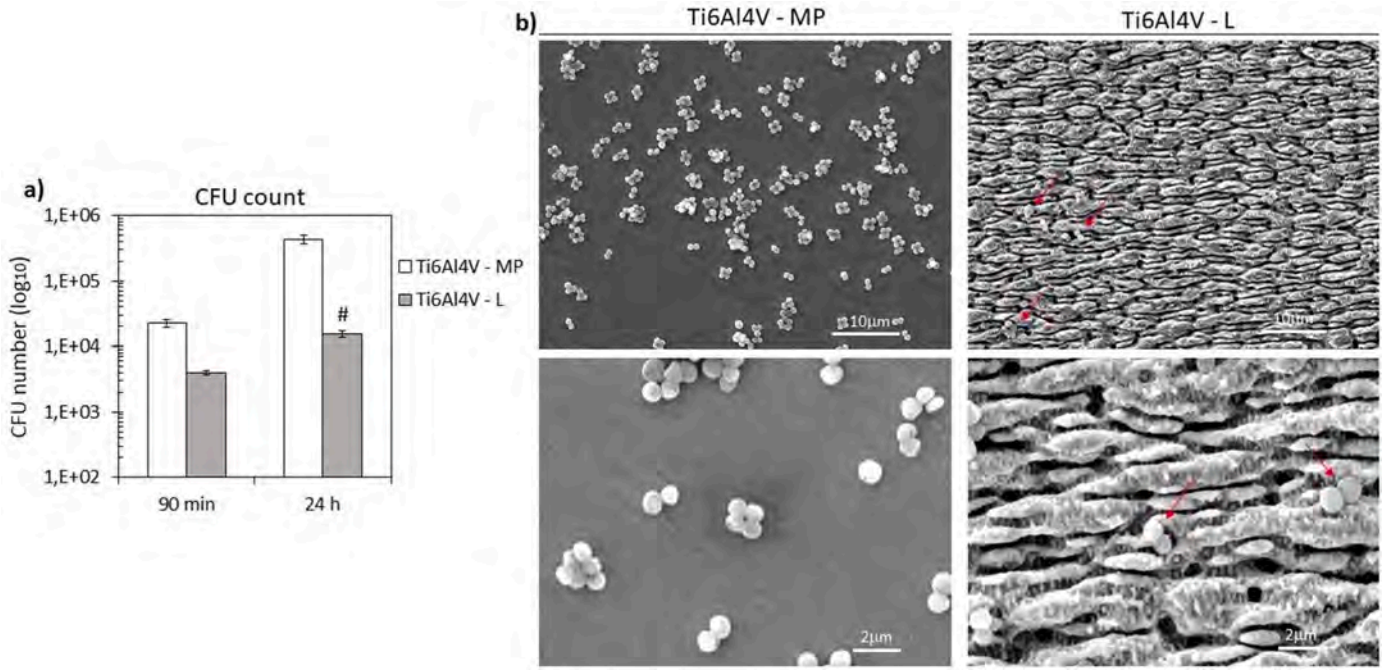

Fig. 6. Antibacterial activity. **(a)** The grooves of the Ti6Al4V – L specimens reduced the number of adhered bacteria in the early adhesion phase (90 min) in comparison to the MP controls; afterward, the number of growing bacteria after 24 h was significantly lower onto Ti6Al4V – L than controls ($p < 0.05$ indicated by #). **(b)** SEM images after 24 h showed the presence of 3D biofilm-like aggregates only onto MP surfaces (left panel), while few single colonies were observed onto laser specimens (right panel). Bars represent means ± dev.st of 3 replicates.

charged groups on the surface. What is the main outcome is that the contact guidance effect on fibroblasts and the anti-adhesive effect on bacteria were coupled on the same surface in this research through laser texturing.

4. Conclusions

Picosecond laser treatment was successfully applied to commercially pure titanium and Ti6Al4V alloy for the obtainment of aligned grooves characterized by micrometric (15–20 μm) width and spacing but sub-micrometric depth (mean roughness not higher than 0.2 μm without significant asperities). Laser treatment induces additional specific micro and sub-micro features on the surface of the grooves, the result is a multi-scale topography of the metallic surface.

Finally, biological characterizations confirmed that the grooves generated by the laser treatment did not induce any cytotoxic effect and they are not a niche for bacteria growth. The treated surfaces were able to guide adhering cells along their orientation by a mechanical contact-guide effect. Moreover, laser texturing was effective in reducing bacterial adhesion and proliferation thanks to a physical burden effect preventing their aggregation into biofilm-like structures.

Declaration of competing interest

The authors declare that they have no known competing financial interests or personal relationships that could have appeared to influence the work reported in this paper.

Appendix A. Supplementary data

Supplementary data to this article can be found online at https://doi.org/10.1016/j.jmrt.2024.03.033.

References

[1] Salmi M. Additive manufacturing processes in medical applications. Materials 2021;14:191. https://doi.org/10.3390/ma14010191.
[2] Ferraris S, Spriano S. Porous titanium by additive manufacturing: a focus on surfaces for bone integration. Metals 2021;11:1343. https://doi.org/10.3390/met11091343.
[3] Schwarz F, Becker J. Treatment of periodontitis and peri-implantitis with an Er: YAG laser: experimental and clinical studies. Med Laser Appl 2005;20:47–59. https://doi.org/10.1016/j.mla.2005.02.005.
[4] Deppe H, Horch H-H, Greim H, Brill T, Wagenpfeil S, Donath K. Peri-implant care with the CO2 laser: in vitro and in vivo results. Med Laser Appl 2005;20:61–70. https://doi.org/10.1016/j.mla.2005.02.002.
[5] Gazott Simões I, Cândido dos Reis A, Lima da Costa Valente M. Analysis of the influence of surface treatment by high-power laser irradiation on the surface properties of titanium dental implants: a systematic review. J Prosthet Dent 2023;6:863–70. https://doi.org/10.1016/j.prosdent.2021.07.026.
[6] Vicente Calazans Neto J, Kreve S, Lima da Costa Valente M, Cândido dos Reis A. Protein absorption on titanium surfaces treated with a highpower laser: a systematic review. J Prosthet Dent 2022. https://doi.org/10.1016/j.prosdent.2022.03.010. in press.
[7] Souza JCM, Sordi MB, Kanazawa M, Ravindran S, Henriques B, Silva FS, Aparicio C, Cooper LF. Nano-scale modification of titanium implant surfaces to enhance osseointegration. Acta Biomater 2019;94:112–31. https://doi.org/10.1016/j.actbio.2019.05.045.
[8] Mendonça G, Mendonça DBS, Aragao FJL, Cooper LF. Advancing dental implant surface technology – from micron to nanotopography. Biomaterials 2008;29:3822–35. https://doi.org/10.1016/j.biomaterials.2008.05.012.
[9] Le Gu′ehennec L, Soueidan A, Layrolle P, Amouriq Y. Surface treatments of titanium dental implants for rapid osseointegration. Dent Mater 2007;23:844–54. https://doi.org/10.1016/j.dental.2006.06.025.
[10] Guo T, Gulati K, Arora H, Han P, Fournier B, Ivanovski S. Race to invade: understanding soft tissue integration at the transmucosal region of titanium dental implants. Dent Mater 2021;37:816–31. https://doi.org/10.1016/j.dental.2021.02.005.
[11] Guo T, Gulati K, Arora H, Han P, Fournier B, Ivanovski S. Orchestrating soft tissue integration at the transmucosal region of titanium implants. Acta Biomater 2021;124:33–49. https://doi.org/10.1016/j.actbio.2021.01.001.
[12] Pye AD, Lockhart DEA, Dawson MP, Murray CA, Smith AJ. A review of dental implants and infection. J Hosp Infect 2009;72:104e110. https://doi.org/10.1016/j.jhin.2009.02.010.
[13] Kumari R, Scharnweber T, Pfleging W, Besser H, Majumdar JD. Laser surface textured titanium alloy (Ti–6Al–4V) – Part II – studies on bio-compatibility. Appl Surf Sci 2015;357:750–8. https://doi.org/10.1016/j.apsusc.2015.08.255.
[14] Kuczy′nska D, Kwa′sniak P, Marczak J, Bonarski J, Smolik J, Garbacz H. Laser surface treatment and the resultant hierarchical topography of Ti grade 2 for

biomedical application. Appl Surf Sci 2016;390:560–9. https://doi.org/10.1016/j.apsusc.2016.08.105.
[15] Rodríguez Á, Trueba P, Amado JM, Tobar MJ, Giner M, Amigó V, Torres Y. Surface modification of porous titanium discs using femtosecond laser structuring. Metals 2020;10:748. https://doi.org/10.3390/met10060748.
[16] Wang S, Zhang M, Liu L, Xu R, Huang Z, Shi Z, Liu J, Li Z, Li X, Hao P, Hao Y. Femtosecond laser treatment promotes the surface bioactivity and bone ingrowth of Ti6Al4V bone scaffolds. Front Bioeng Biotechnol 2022;10:962483. https://doi.org/10.3389/fbioe.2022.962483.
[17] Papa S, Abou Khalil A, Hamzeh-Cognasse H, Thomas M, Maalouf M, Di Maio Y, Sedao X, Guignandon A, Dumas V. Dual-functionalized titanium by ultrafast laser texturing to enhance human gingival fibroblasts adhesion and minimize Porphyromonas gingivalis colonization. Appl Surf Sci 2022;606:154784. https://doi.org/10.1016/j.apsusc.2022.154784.
[18] Cunha A, Elie A-M, Plawinski L, Serro AP, Botelho do Rego AM, Almeida A, Urdaci MC, Durrieu M-C, Vilar R. Femtosecond laser surface texturing of titanium as a method to reduce the adhesion of Staphylococcus aureus and biofilm formation. Appl Surf Sci 2016;360:485–93. https://doi.org/10.1016/j.apsusc.2015.10.102.
[19] https://www. https://www.geass.it/en/synthegra (accessed 20 November 2023).
[20] Thomsson M, esposito M. A retrospective case series evaluating Branemark BioHelix implants placed in a specialist private practice following 'conventional' procedures. One-year results after placement. Eur J Oral Implant 2008;1:229–34.
[21] BioHorizons. Laser-lok clinical overview. 2017. p. 1–56. https://vsr.biohorizons.com/GetDocument?DocumentId=43809. [Accessed 17 November 2023].
[22] Frijd V, Linderback P, Wennerberg A, de Paz LC, Svensater G, Davies JR. Effect of nanoporous TiO2 coating and anodized Ca2+ modification of titanium surfaces on early microbial biofilm formation. BMC Oral Health 2011;11:8. https://doi.org/10.1186/1472-6831-11-8.
[23] Quirynen M, Bollen CML, Papaioannou W, Van Eldere J, van Steenberghe D. The influence of titanium abutment surface roughness on plaque accumulation and gingivitis: short term observations. Int J Oral Maxillofac Implants 1996;11:69–178.
[24] Al-Ahmad A, Wiedmann-Al-Ahmad M, Fackler A, Follo M, Hellwig E, Bächle M, Hannig C, Han J-S, Wolkewitz M, Kohal R. In vivo study of the initial bacterial adhesion on different implant materials. Arch Oral Biol 2013;58:1139–47.
[25] Curry EC, Hart RG, Habtu DY, Chamberlain NR. Detection and partial characterization of extracellular inducers of persistence in Staphylococcus epidermidis and Staphylococcus aureus. J Med Microbiol 2021;70. https://doi.org/10.1099/jmm.0.001392. PMID: 34170218.
[26] Ferraris S, Cochis A, Cazzola M, Tortello M, Scalia A, Spriano S, Rimondini L. Cytocompatible and anti-bacterial adhesion nanotextured titanium oxide layer on titanium surfaces for dental and orthopedic implants. Front Bioeng Biotechnol 2019;7:103. https://doi.org/10.3389/fbioe.2019.00103. 2019.
[27] John AK, Schmaler M, Khanna N, Landmann R. Reversible daptomycin tolerance of adherent staphylococci in an implant infection model. Antimicrob Agents Chemother 2011;55:3510–6. https://doi.org/10.1128/AAC.00172-11.
[28] Nowakowska J, Griesser HJ, Textor M, Landmann R, Khanna N. Antimicrobial properties of 8-hydroxyserrulat-14-en-19-oic acid for treatment of implant-associated infections. Antimicrob Agents Chemother 2013;57:333–42. https://doi.org/10.1128/AAC.01735-12.
[29] Tahaei SA Senobar, Stájer A, Barrak I, Ostorházi E, Szabó D, Gajdács M. Correlation between biofilm-formation and the antibiotic resistant phenotype in Staphylococcus aureus isolates: a laboratory-based study in Hungary and a review of the literature. Infect Drug Resist 2021;23:1155–68. https://doi.org/10.2147/IDR.S303992.
[30] Bygd HC, Forsmark KD, Bratlie KM. Altering in vivo macrophage responses with modified polymer properties. Biomaterials 2015;56:187–97. https://doi.org/10.1016/j.biomaterials.2015.03.042. Epub 2015 Apr 17. PMID: 25934291.
[31] Gadelmawla ES, Koura MM, Maksoud TMA, Elewa M, Soliman HH. Roughness parameters. J Mater Process Technol 2002;123:133–45. https://doi.org/10.1016/S0924-0136(02)00060-2.
[32] Donaghy CL, McFadden R, Smith GC, Kelaini S, Carson L, Malinov S, Margariti A, Chan C-W. Fibre laser treatment of beta TNZT titanium alloys for load-bearing implant applications: effects of surface physical and chemical features on mesenchymal stem cell response and Staphylococcus aureus bacterial attachment. Coatings 2019;9:186. https://doi.org/10.3390/coatings9030186.
[33] Ferraris S, Warchomicka F, Iranshahi F, Rimondini L, Cochis A, Spriano S. Electron beam structuring of Ti6Al4V: new insights on the metal surface properties influencing the bacterial adhesion. Materials 2020;13:409. https://doi.org/10.3390/ma13020409.
[34] Ferraris S, Warchomicka F, Ramskogler C, Tortello M, Cochis A, Scalia A, Gautier di Confiengo G, Keckes J, Rimondini L, Spriano S. Surface structuring by Electron Beam for improved soft tissues adhesion and reduced bacterial contamination on Ti-grade 2. J Mater Process Technol 2019;266:518–29. https://doi.org/10.1016/j.jmatprotec.2018.11.026.
[35] Mekayarajjananonth T, Winkler S. Contact angle measurement on dental implant biomaterials. J Oral Implantol 1999;25:230–6. https://doi.org/10.1563/1548-1336(1999)025<0230:CAMODI>2.3.CO;2.
[36] Lim YJ, Oshida Y, Andres CJ, Barco MT. Surface characterizations of variously treated titanium materials. Int J Oral Maxillofac Implants 2001;16:333–42.
[37] Ferraris S, Yamaguchi S, Barbani N, Cristallini C, Gautier di Confiengo G, Barberi J, Cazzola M, Miola M, Vernè E, Spriano S. The mechanical and chemical stability of the interfaces in bioactive materials: the substrate-bioactive surface layer and hydroxyapatite bioactive surface layer interfaces. Mater Sci Eng C 2020;116:1112.
[38] Bal BS, Rahaman MN. Orthopedic applications of silicon nitride ceramics. Acta Biomater 2012;8:2889–98. https://doi.org/10.1016/j.actbio.2012.04.031.
[39] Kosmulski M. Ph dependent surface charging and point of zero charge. IV. Update and new approach. J Colloid Interface Sci 2009;337:439–48. https://doi.org/10.1016/j.jcis.2009.04.072.
[40] Luxbacher T. The ZETA guide principles of the streaming potential technique. Anton Paar; 2014.
[41] Vinhas AS, Aroso C, Salazar F, López-Jarana P, Ríos-Santos JV, Herrero-Climent M. Review of the mechanical behavior of different implant-abutment connections. Int J Environ Res Publ Health 2020;17:8685. https://doi.org/10.3390/ijerph17228685.
[42] Tanner A, Maiden MF, Lee K, Shulman LB, Weber HP. Dental implant infections. Clin Infect Dis 1997;25:13–7. https://doi.org/10.1086/516243.
[43] Shah FA, Trobos M, Thomsen P, Palmquist A. Commercially pure titanium (cp-Ti) versus titanium alloy (Ti6Al4V) materials as bone anchored implants — is one truly better than the other? Mater Sci Eng C 2016;62:960–6. https://doi.org/10.1016/j.msec.2016.01.032.
[44] Wennerberg A, Sennerby L, Kultje C, Lekholm U. Some soft tissue characteristics at implant abutments with different surface topography. A study in humans. J Clin Periodontol 2003;30:88–94. https://doi.org/10.1034/j.1600-051x.2003.10026.x.
[45] Ghinassi B, Di Baldassarre A, D'Addazio G, Traini T, Andrisani M, Di Vincenzo G, Gaggi G, Piattelli M, Caputi S, Sinjari B. Gingival response to dental implant: comparison study on the effects of new nanopored laser-treated vs. Traditional healing abutments. Int J Mol Sci 2020;21:6056. https://doi.org/10.3390/ijms21176056.
[46] George PM, Lyckman AW, LaVan DA, Hegde A, Leung Y, Avasare R, Testa C, Alexander PM, Langer R, Sur M. Fabrication and biocompatibility of polypyrrole implants suitable for neural prosthetics. Biomaterials 2005;26:3511–9. https://doi.org/10.1016/j.biomaterials.2004.09.037.
[47] Mustafa K, Odén A, Wennerberg A, Hultenby K, Arvidson K. The influence of surface topography of ceramic abutments on the attachment and proliferation of human oral fibroblasts. Biomaterials 2005;26:373–81. https://doi.org/10.1016/j.biomaterials.2004.02.037.
[48] Costa RC, Nagay BE, Bertolini M, Be Costa-Oliveira AA Sampaio, Retamal-Valdes B, Shibli JA, Feres M, Barão VAR, Jgs Souza. Fitting pieces into the puzzle: the impact of titanium-based dental implant surface modifications on bacterial accumulation and polymicrobial infections. Adv Colloid Interface Sci 2021;298:102551. https://doi.org/10.1016/j.cis.2021.102551.
[49] Trehan RS, McDonnell EP, Jv McCoy PA Ohman-Strickland, Donovan C, Quinoa TR, Morrison DS. Comparing the quantitative fit-testing results of half-mask respirators with various skin barriers in a crossover study design: a pilot study. J Hosp Infect 2021;111:125–31. https://doi.org/10.1016/j.jhin.2021.02.010.
[50] Creugers NH, Kreulen CM, Snoek PA, de Kanter RJ. A systematic review of single-tooth restorations supported by implants. J Dent 2000;28:209–17. https://doi.org/10.1016/s0736-5748(99)00078-7.
[51] Ferraris S, Venturello A, Miola M, Cochis A, Rimondini L, Spriano S. Antibacterial and bioactive nanostructured titanium surfaces for bone integration. Appl Surf Sci 2014;311:279–91. https://doi.org/10.1016/j.apsusc.2014.05.056.
[52] Sorzabal-Bellido I, Barbieri L, Beckett AJ, Prior IA, Susarrey-Arce A, Tiggelaar RM, Fothergill J, Raval R, Diaz Fernandez YA. Effect of local topography on cell division of Staphylococcus spp. Nanomaterials 2022;12:683. https://doi.org/10.3390/nano12040683.
[53] Lazzini G, Romoli L, Lutey AHA, Fuso F. Modelling the interaction between bacterial cells and laser-textured surfaces. Surf Coating Technol 2019;375:8–14. https://doi.org/10.1016/j.surfcoat.2019.06.078.